predicted targets. If these genes are miRNA targets in the gonadal pathway, then their down-regulation should restore longevity to *mir-84;mir-241;glp-1* triple mutants. RNAi treatment from L4 onwards revealed that only *lin-14RNAi* restored life-span extension to the triple mutants (Fig. 4A and table S1).

lin-14 is an intriguing candidate because Slack had previously shown that *lin-14* loss of function extends life span in a *daf-16*/FOXO–dependent manner, and *lin-14* gain-of-function mutations shorten life span (*20*). During development *lin-14* governs L1-L2 transitions, but its context in aging is unclear. We found that *lin-14RNAi* extended life span in WT animals as reported, but it did not further extend the life of *glp-1* mutants (Fig. 4A). To examine its relationship with *daf-16*/FOXO, we tested whether *lin-14* knockdown influenced *daf-16* target gene expression. Similar to aging experiments in which longevity was restored, *lin-14RNAi* also significantly restored *daf-16* expression of *sod-3* and *lipl-4* to *mir-84;mir-241;glp-1* (Fig. 4F and fig. S7F). Altogether, these observations suggest that the miRNAs down-regulate *lin-14* and promote longevity via *daf-16*.

To test this hypothesis, we examined regulation of *lin-14* by *mir-84;mir-241*. As above, a luciferase reporter with the *lin-14*-3′UTR was down-regulated by miRNAs (fig. S7B). Similarly, a *lin-14-3'UTR-DR* construct was up-regulated in *mir-84;mir-241* double mutants relative to WT, whereas the *unc-1-3'UTR-DR* controls were unchanged (Fig. 4, B and C). Consistent with a role in the gonadal pathway, the *lin-14-3'UTR-DR* construct and full-length *lin-14::gfp* were down-regulated in intestinal nuclei of germline-less animals relative to gonad-intact controls (Fig. 4, D and E, and fig. S7, D and E). Collectively, these results reveal that *lin-14*, a core component of the developmental clock, functions in the gonadal longevity circuit, where it is down-regulated by miRNAs upon germline removal.

In this work, we show that components of an early life developmental timing switch (i.e., the steroid receptor DAF-12; its ligands; its target miRNAs of the *let-7* family; and LIN-14, the miRNAs' target) are used to regulate adult life span in response to signals from the gonad. We propose a model in which they work as part of a hormone-regulated switch between reproductive and survival modes at larval to adult stage commitments (fig. S8). When GSC proliferation is prevented, unknown signals up-regulate *daf-36* and DA production by the L4/young adult stage, subsequently activating DAF-12 and its miRNA targets, *mir-84* and *mir-241*. In turn, these miRNAs down-regulate *akt-1*, *lin-14*, and possibly other targets, which stimulate DAF-16/FOXO transcriptional activity, extending survival and life span. Because miRNA deletion does not fully abolish DAF-16 activity, other signals from either gonad or DAF-12 may also prompt gonadal longevity. Conversely, when GSC proliferation ensues, DA signaling is down-regulated, miRNA expression is low, and *lin-14* and *akt-1* expression are high, resulting in normal life span. This switch could provide a critical link between development and longevity, serving as a checkpoint monitoring the state of the germ line. For example, germline absence could mimic endogenous stress signals induced by germline quiescence or proliferative arrest in response to nutrient deprivation, infection, or damage. As components of a developmental timer, the hormone-miRNA axis could ensure coordinate metabolism, maturation, and the relative timing of events between the reproductive system and the soma, with ultimate effects on life span. It will be interesting to dissect the interaction of other miRNAs implicated in longevity with this axis (*20*, *21*). Furthermore, these findings extend the role of *let-7* family members beyond developmental timing and differentiation to the regulation of insulin/IGF signaling and metabolism, similar to recent studies in mammals (*22*). Because *let-7* family members and other components of this circuitry are evolutionarily conserved, it will be interesting to see if similar pathways affect longevity in vertebrates.

References and Notes

1. H. Hsin, C. Kenyon, *Nature* **399**, 362 (1999).
2. N. Arantes-Oliveira, J. Apfeld, A. Dillin, C. Kenyon, *Science* **295**, 502 (2002).
3. T. Flatt *et al*., *Proc. Natl. Acad. Sci. U.S.A.* **105**, 6368 (2008).
4. B. Gerisch *et al*., *Proc. Natl. Acad. Sci. U.S.A.* **104**, 5014 (2007).
5. T. M. Yamawaki *et al*., *PLoS Biol.* **8**, e1000468 (2010).
6. J. R. Berman, C. Kenyon, *Cell* **124**, 1055 (2006).
7. M. McCormick, K. Chen, P. Ramaswamy, C. Kenyon, *Aging Cell* **11**, 192 (2012).
8. J. Wollam *et al*., *PLoS Biol.* **10**, e1001305 (2012).
9. J. Wollam *et al*., *Aging Cell* **10**, 879 (2011).
10. T. Yoshiyama-Yanagawa *et al*., *J. Biol. Chem.* **286**, 25756 (2011).
11. A. Bethke, N. Fielenbach, Z. Wang, D. J. Mangelsdorf, A. Antebi, *Science* **324**, 95 (2009).
12. C. M. Hammell, X. Karp, V. Ambros, *Proc. Natl. Acad. Sci. U.S.A.* **106**, 18668 (2009).
13. J. Goudeau *et al*., *PLoS Biol.* **9**, e1000599 (2011).
14. M. C. Wang, E. J. O'Rourke, G. Ruvkun, *Science* **322**, 957 (2008).
15. L. R. Lapierre, S. Gelino, A. Meléndez, M. Hansen, *Curr. Biol.* **21**, 1507 (2011).
16. M. Hammell *et al*., *Nat. Methods* **5**, 813 (2008).
17. C. J. Kenyon, *Nature* **464**, 504 (2010).
18. S. Paradis, G. Ruvkun, *Genes Dev.* **12**, 2488 (1998).
19. T. D. Resnick, K. A. McCulloch, A. E. Rougvie, *Dev. Dyn.* **239**, 1477 (2010).
20. M. Boehm, F. Slack, *Science* **310**, 1954 (2005).
21. K. Boulias, H. R. Horvitz, *Cell Metab.* **15**, 439 (2012).
22. H. Zhu *et al*., *Cell* **147**, 81 (2011).

Acknowledgments: We thank C. Montino for technical help; M. Denzel for manuscript comments; S. Lo (Chang-Qung University) for plasmids; and I. Greenwald (Columbia University), H. Aguilaniu (ENS de Lyon), C. Kenyon (University of California San Francisco), and the Caenorhabditis Genetics Center for strains. This work was supported by an European Molecular Biology Organization fellowship (Y.S.) and the National Institute on Aging/NIH, the Ellison Medical Foundation, the Max Planck Society, Sybacol/Bundesministerium für Bildung und Forschung, and CECAD (A.A.). Strain *pha-1*(*e2123*);arEx1273(*lin-14::gfp*) is available from Iva Greenwald (Columbia University) subject to a materials transfer agreement with the Howard Hughes Medical Institute.

Supplementary Materials

www.sciencemag.org/cgi/content/full/338/6113/1472/DC1
Materials and Methods
Figs. S1 to S8
Tables S1 to S3
References (*23*–*28*)

16 August 2012; accepted 5 November 2012
10.1126/science.1228967

Hox Genes Regulate Digit Patterning by Controlling the Wavelength of a Turing-Type Mechanism

Rushikesh Sheth,[1]*† Luciano Marcon,[2,3]* M. Félix Bastida,[1,4] Marisa Junco,[1] Laura Quintana,[2,3] Randall Dahn,[5] Marie Kmita,[6]‡ James Sharpe,[2,3,7]‡ Maria A. Ros[1,4]‡

The formation of repetitive structures (such as stripes) in nature is often consistent with a reaction-diffusion mechanism, or Turing model, of self-organizing systems. We used mouse genetics to analyze how digit patterning (an iterative digit/nondigit pattern) is generated. We showed that the progressive reduction in *Hoxa13* and *Hoxd11-Hoxd13* genes (hereafter referred to as distal *Hox* genes) from the *Gli3*-null background results in progressively more severe polydactyly, displaying thinner and densely packed digits. Combined with computer modeling, our results argue for a Turing-type mechanism underlying digit patterning, in which the dose of distal *Hox* genes modulates the digit period or wavelength. The phenotypic similarity with fish-fin endoskeleton patterns suggests that the pentadactyl state has been achieved through modification of an ancestral Turing-type mechanism.

Digit patterning has commonly been interpreted in the context of a morphogen gradient model (*1*, *2*). The proposed morphogen Sonic hedgehog (Shh) emanates from the zone of polarizing activity (a cluster of mesodermal cells in the posterior border of

the limb bud) and establishes a gradient with maximum levels posteriorly. Gli3 is the major mediator of Shh signaling in limb development and a genetic cause of polydactyly (*2*). Because Shh prevents the processing of Gli3 to its repressor form (Gli3R), the Shh gradient is translated into an inverse gradient of Gli3R (*3*, *4*). The surprising finding that mouse *Gli3* and *Shh*;*Gli3* null mutants display identical polydactylous limb phenotypes demonstrates that an iterative series of digits can form in the absence of Shh (*4*, *5*). Rather than supporting a gradient model, this observation is consistent with a Turing-type model for digit patterning (*6*–*11*) in which dynamic interactions between activator and inhibitor molecules determine the wavelength of the specific pattern and produce periodic patterns of spots or stripes. This pattern has been hypothesized to act as a molecular prepattern for chondrogenesis. According to one of the specific predictions of the model, the digit period or wavelength, defined as the combined thickness of both digit and interdigital region, should be subject to modulation by perturbing the correct parameter of the gene network. This should lead to autopods with digits varying in thickness and number, which has never been clearly observed to date.

Although the core molecules of a self-organizing mechanism remain unknown, potential candidates for molecular modulators of the system include the *Hox* genes (*10*, *12*). Distal *Hoxa* and *Hoxd* genes have a well-documented impact on digit number (*13*), though their specific role remains unclear, possibly due to their various interactions with the Shh-Gli3 pathway. These interactions include the mutual transcriptional regulation between *Hox* genes and *Shh* and the binding of Hoxd12 to Gli3R, resulting in a blockage of Gli3R repressor activity (*14*–*16*). In general, gain- and loss-of-function experiments suggest a positive relation between *Hox* genes and digit number (*14*, *17*–*22*), which is also indicated by the ectopic anterior up-regulation of distal *Hoxd* genes in the *Gli3*-dependent polydactyly (*4*, *5*). However, we showed that the combined deletion of *Hoxd11-13* and *Gli3* exacerbated the *Gli3* polydactyly (*23*), suggesting instead a negative relation between distal *Hoxd* genes and digit number.

Hoxd11-13;*Gli3* mutants displayed a gain of *Hoxa13* expression, similar to *Gli3* mutants (*23*). To address the relation between *Hoxa13* and digit number, we generated double *Hoxa13*;*Gli3* mutants (see supplementary materials and methods). At embryonic day 12.5 (E12.5), *Sox9* expression marked the five digital chondrogenic condensations in control autopods and revealed the delay in differentiation in the anterior mesoderm and the polydactyly typical of the *Gli3* deficiency (Fig. 1A) (*24*). $Hoxa13^{-/-};Gli3^{Xtj/Xtj}$ showed seven to eight digital condensations in the posterior mesoderm plus a diffuse *Sox9* expression in the anterior mesoderm, which likely corresponded to presumptive digital condensations (Fig. 1A). Even though the number of digits could not be precisely determined, *Sox9* expression suggested an increase in digit number in $Hoxa13^{-/-};Gli3^{Xtj/Xtj}$ compared with $Gli3^{Xtj/Xtj}$ mutants, supporting a negative effect of *Hoxa13* on digit number, similar to distal *Hoxd* genes (*23*).

$Hoxa13^{-/-};Gli3^{Xtj/Xtj}$ limbs also displayed reduced digit wavelength and digit bifurcations (Fig. 1A). To quantify both features, we analyzed curved anterior posterior (AP) profiles of *Sox9* expression at four equidistant positions along the proximal distal (PD) axis of the digit region of the *Hoxa13*;*Gli3* mutants shown in Fig. 1A (Fig. 1B and supplementary materials). We measured the average digit period and AP length of each profile (shown in

[1]Facultad de Medicina, Instituto de Biomedicina y Biotecnología de Cantabria, Consejo Superior de Investigaciones Científicas–Sociedad para el Desarrollo Regional de Cantabria–Universidad de Cantabria, 39011 Santander, Spain. [2]European Molecular Biology Laboratory (EMBL)–Centre for Genomic Regulation (CRG) Systems Biology Research Unit, CRG, Doctor. Aiguader 88, 08003 Barcelona, Spain. [3]Universitat Pompeu Fabra, 08003 Barcelona, Spain. [4]Departamento de Anatomía y Biología Celular, Universidad de Cantabria, 39011 Santander, Spain. [5]7322 Countrywood Lane, Madison, WI 53719, USA. [6]Institut de Recherches Cliniques de Montréal, Université de Montréal, Montréal, Québec H2W 1R7, Canada. [7]Institució Catalana de Recerca i Estudis Avançats, Passeig Lluís Companys 23, 08010 Barcelona, Spain.

*These authors contributed equally to this work.
†Present address: Institut de Recherches Cliniques de Montréal, University of Montréal, Montréal, Québec, Canada.
‡To whom correspondence should be addressed. E-mail: marian.ros@unican.es (M.A.R.); james.sharpe@crg.eu (J.S.); marie.kmita@ircm.qc.ca (M.K.)

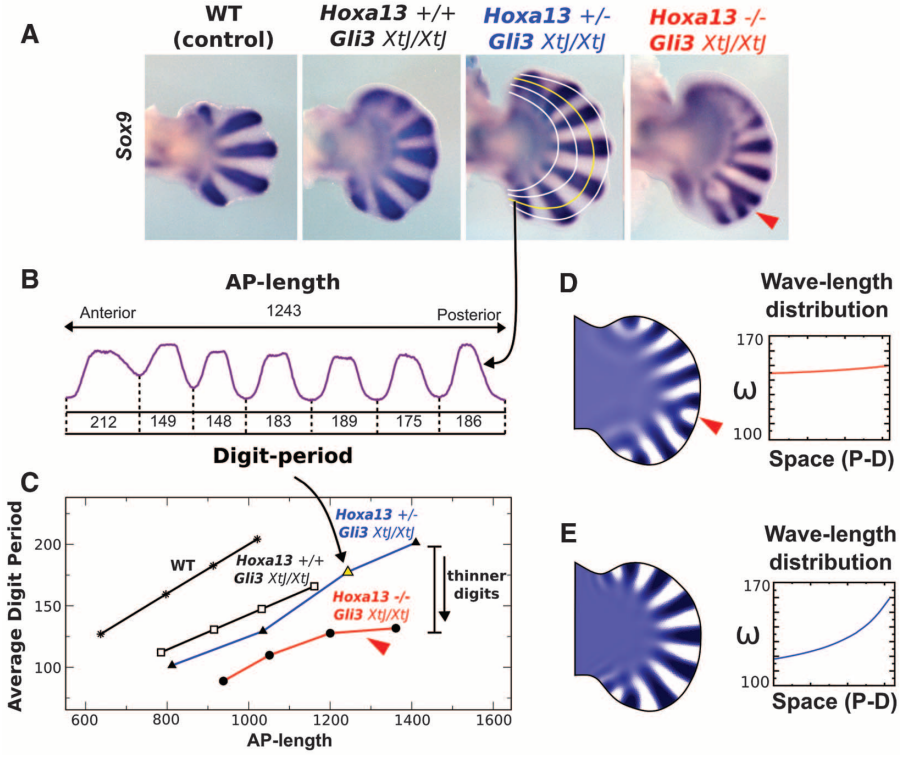

Fig. 1. (**A**) Expression of *Sox9* in E12.5 limbs of the *Hoxa13;Gli3* allelic series. Note the delayed differentiation in the anterior mesoderm in the absence of *Gli3*. The curved white and yellow lines show the AP profiles used for the analysis of *Sox9*. The red arrowhead points to a digit bifurcation. WT, wild type. (**B**) *Sox9* staining intensity along the yellow profile indicated by the curved arrow. AP length and the period of each digit (from minimum to minimum) are measured and shown for $Hoxa13^{+/-};Gli3^{Xtj/Xtj}$. (**C**) Chart showing the average digit periods versus AP lengths for each profile and limb. A linear relation is observed in controls and in the $Gli3^{Xtj/Xtj}$ background for either the normal or heterozygous dose of *Hoxa13*, whereas a flatter relation that correlates with bifurcations (red arrowhead) is observed in the $Hoxa13^{-/-};Gli3^{Xtj/Xtj}$ limbs (red line). The curved arrow marks the yellow point corresponding to the profile in (B). (**D** and **E**) Two simulations of the reaction-diffusion model inside an E12.5 *Gli3* mutant limb shape. (D) The activator concentration obtained in the simulation with a uniform modulation of wavelength ω (shown in the graph) shows digit bifurcation (red arrowhead) similar to the $Hoxa13^{-/-}Gli3^{Xtj/Xtj}$ mutants. (E) The simulation result when wavelength is modulated according to a suitable PD gradient (in this case, a 2D gradient of simulated FGF signaling activity) avoids bifurcations, because the wavelength increases with increasing AP length. Limbs shown in all figures are forelimbs with distal to the right and anterior to the top.

Fig. 1B for *Hoxa13*$^{+/-}$;*Gli3*$^{XtJ/XtJ}$) and plotted results (Fig. 1C). In control, *Hoxa13*$^{+/+}$;*Gli3*$^{XtJ/XtJ}$, and *Hoxa13*$^{+/-}$;*Gli3*$^{XtJ/XtJ}$ mutants, the average digit period increased along the PD axis, whereas the ratio between the average digit period and the AP length was constant, suggesting that the wavelength of a Turing-type mechanism was scaled along the PD axis to maintain a constant number of digits. However, this was not true for

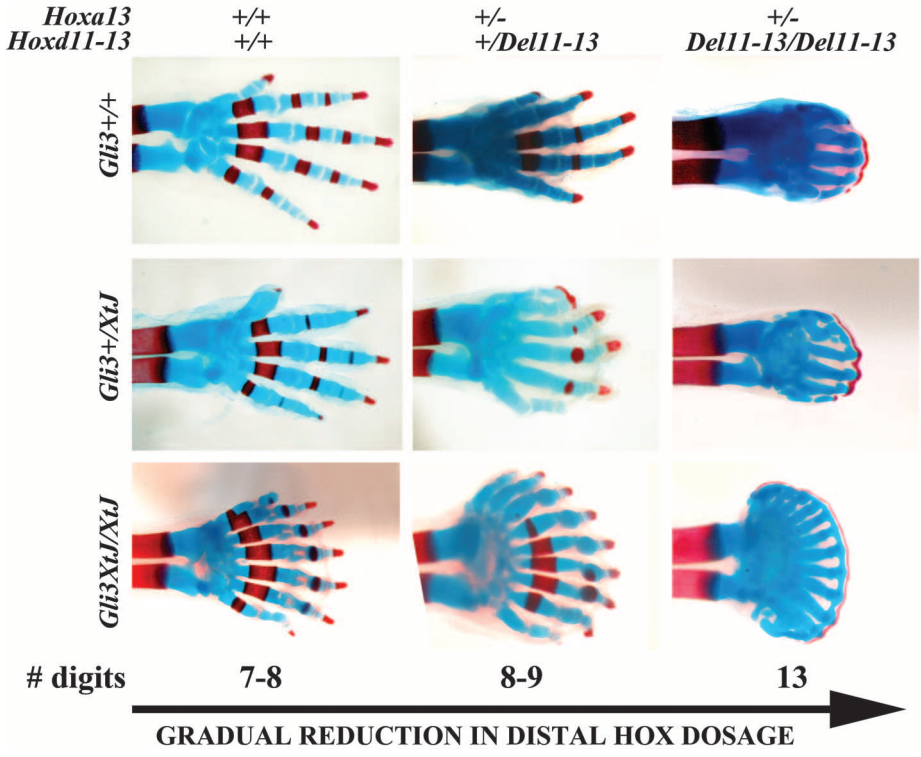

Fig. 2. Representative skeletal phenotypes of newborns of the *Hoxa13;Hoxd11-13;Gli3* allelic series. Digit number (indicated for the *Gli3*$^{XtJ/XtJ}$ condition) increases as distal *Hox* dose is reduced. When only one functional copy of *Hoxa13* remains (right column), the tip of the digits is connected by a continuous band of ossified (red) and cartilaginous (blue) tissue rimming the distal border of the limb and becoming more conspicuous as *Gli3* copies are removed.

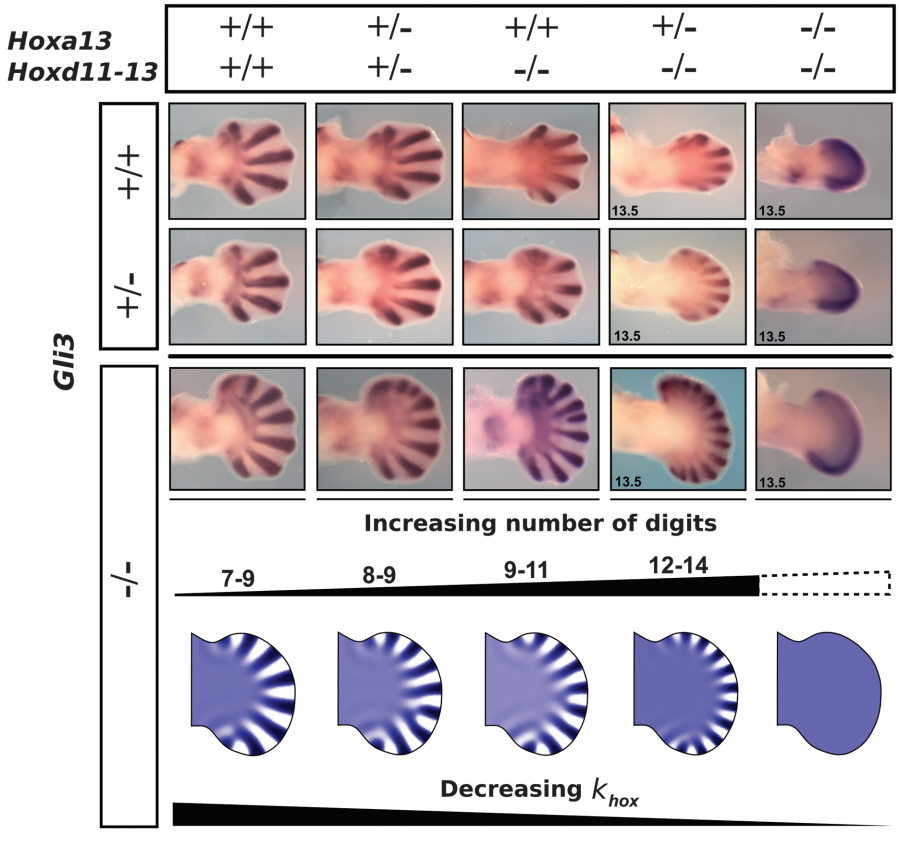

Fig. 3. The phenotypes of triple mutants can be replicated by the Turing model. (**Top**) The first three rows show *Sox9* expression at E12.5 and E13.5 for different combinations of the triple *Hoxa13;Hoxd11-13;Gli3* allelic series. As more *Hox* are removed, the general trend shows an increase in digit number and a decrease in digit thickness. The trend is most strongly evident in the complete absence of *Gli3* (third row). (**Bottom**) A similar behavior is shown by the reaction-diffusion simulations, where a decrease of the PD gradient used to modulate wavelength is correlated with reduced *Hox* dose (k_{hox}). Additionally, the model predicts a narrower digital region along the PD axis, which eventually shrinks to zero, and no pattern is formed.

the *Hoxa13*$^{-/-}$;*Gli3*$^{XtJ/XtJ}$ limbs, where the average digit period flattened off distally, and, in agreement with a Turing-type mechanism, digit bifurcations occurred as the AP length increased (Fig. 1A). Our quantification suggested that normal digit patterning involves an effective PD increase of the digit wavelength, which we hypothesized must be carefully controlled if bifurcations are to be avoided.

To test this hypothesis, we built a two-dimensional (2D) finite-element model based on the shape of the *Gli3*$^{XtJ/XtJ}$ handplate at E12.5 and simulated a reaction-diffusion system by scaling the wavelength in either a uniform (remaining constant) or a graded manner along the PD axis of the digital region (Fig. 1, D and E , and supplementary text). We used a generic activator-inhibitor reaction-diffusion system, employing the minimal conditions to satisfy Turing instability (see supplementary text) (*25*). We determined whether a single reaction parameter of the model could be an effective target for wavelength modulation (figs. S4 and S5) and chose the effect of activator on inhibitor production (g_u) as the most suitable (see supplementary text). Our simulations showed that digit bifurcations occurred in the uniform case (red arrowhead Fig. 1D), whereas no bifurcations were shown when we used graded wavelength scaling (Fig. 1E), reproducing the observed mutant patterns. Our model suggests that, in the absence of *Gli3*, the genetic reduction of *Hoxa13* produces a global reduction in wavelength (ω), thereby increasing digit number, but also causes a shallower PD gradient of ω, which explains the observed digit bifurcations. Because there is no evidence for a PD-graded *Hox* expression, the simplest interpretation of the model is that ω is modulated by both the *Hoxa13* gene (explaining the global reduction in wavelength) and fibroblast growth factor (FGF) signaling (explaining the PD gradient), possibly by co-regulating the same target genes (see supplementary text).

Because *Hoxa13*$^{-/-}$;*Gli3*$^{XtJ/XtJ}$ double mutants display ectopic anterior expression of *Hoxd12* and *Hoxd13*, similar to *Gli3* mutants (fig. S1), it remained possible that the increased polydactyly was due to the gain of *Hoxd12* and *Hoxd13*. To challenge such functional compensation and test whether the cumulative sum of distal functional *Hox* genes controls digit number by modulating the digit period, we generated triple mutants carrying the *Hoxa13*$^{-}$, *Hoxd*$^{Del11\text{-}13}$, and *Gli3*^{XtJ} alleles (Fig. 2). Skeletal preparations of neonates of the triple-mutant allelic series showed a variety of patterning defects, including syndactyly (fused digits), brachydactyly (shortened digits), absence of joints, ventral bending of digits, and delayed ossification. Most salient, however, was the clear trend toward increased digit number as progressively more alleles of distal *Hox* genes were removed in the

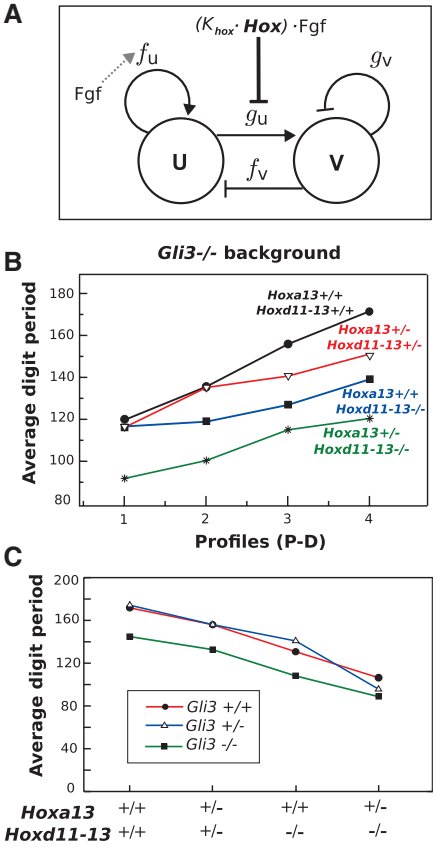

Fig. 4. (**A**) Schematic representation of the network of a general activator-inhibitor Turing model. The four reaction kinetic parameters are shown: f_u, f_v, g_u, and g_v. Fgf promotes a PD-graded distribution of the parameter f_u to drive stripe orientation (gray dashed arrow). Hox and Fgf inhibit the parameter g_u to increase the wavelength in a PD-graded manner (bold line). U, activator; V, inhibitor. (**B**) Graphs of the average digit period of the triple mutants with *Gli3*$^{-/-}$ background at four equidistant positions along the PD axis of the digital region. With the exception of *Hoxa13*$^{+/-}$;*Hoxd*$^{Del11\text{-}13/Del11\text{-}13}$;*Gli3*$^{Xtj/Xtj}$, a clear trend is observed: The PD gradient of wavelength is generally shallower as distal *Hox* genes are removed. (**C**) Graphs of average digit period (wavelength) versus distal *Hox* gene dose in the three different *Gli3* backgrounds. A smooth positive correlation between *Hox* gene dose and wavelength is observed in all three cases.

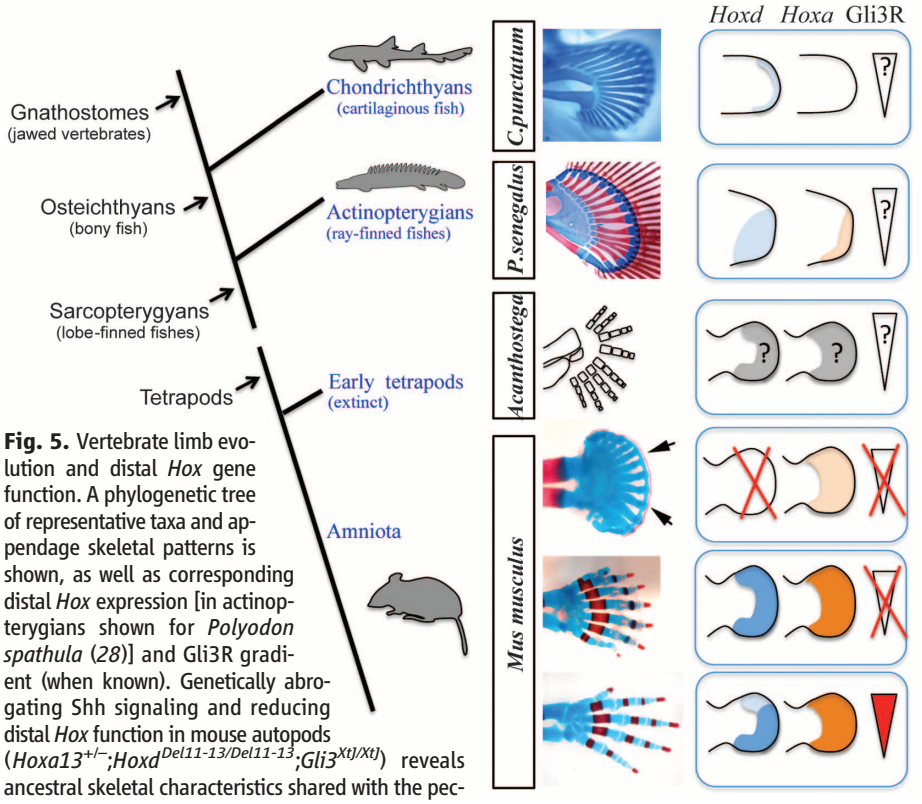

Fig. 5. Vertebrate limb evolution and distal *Hox* gene function. A phylogenetic tree of representative taxa and appendage skeletal patterns is shown, as well as corresponding distal *Hox* expression [in actinopterygians shown for *Polyodon spathula* (*28*)] and Gli3R gradient (when known). Genetically abrogating Shh signaling and reducing distal *Hox* function in mouse autopods (*Hoxa13*$^{+/-}$;*Hoxd*$^{Del11\text{-}13/Del11\text{-}13}$;*Gli3*$^{Xtj/Xtj}$) reveals ancestral skeletal characteristics shared with the pectoral fins of sharks (*Chiloscyllium punctatum*) and primitive ray-finned fishes (*Polypterus senegalus*): numerous, densely packed, and iterative elements, with a distal cartilaginous band corresponding to the distal radials of fish fins (arrows). The periodic pattern of skeletal elements evident in fins and mutant limbs strongly suggests that a self-organizing Turing-type mechanism of chondrogenesis is deeply conserved in vertebrate phylogeny. Our results further indicate that distal *Hox* gene dose regulates the number and spacing of skeletal elements formed, implicating distal *Hox* gene regulatory networks as critical drivers of the evolution of the pentadactyl limb.

absence of *Gli3* (Fig. 2). The number of digits increased from 7 to 9 (typical of $Gli3^{XtJ/XtJ}$) to 8 to 9 when one functional allele of both *Hoxa13* and *Hoxd11-13* was removed; further, to 9 to 11 when both *Hoxd11-13* alleles were removed (*23*); and, finally, to at least 12 to 14 digits when only one copy of *Hoxa13* remained ($Hoxa13^{+/-}$;$Hoxd^{Del11\text{-}13/Del11\text{-}13}$;$Gli3^{XtJ/XtJ}$) (Fig. 2). The midgestational lethality of *Hoxa13* homozygous mutants precluded their analysis at this stage. The increase in digit number as distal *Hox* genes were removed did not rely on increased AP handplate size, as in *Gli3* single mutants (*26*), but rather on a reduced wavelength as digits were thinner and had narrower gaps between them, while remaining regularly spaced (Figs. 1A and 2). These phenotypes cannot be explained by a model of positional information based on a morphogen gradient.

To compare the principal phenotypes of the triple allelic series with our computational model, we analyzed *Sox9* expression at E12.5, when the condensations are being laid down and the Turing mechanism should be operative. Quantification of these mutants confirmed that there was no strict correlation between the progressive increase in digit number and handplate size, which instead coincided with thinner, more densely packed digits (Fig. 3). In our computer model, both Hox levels and FGF signaling contribute to wavelength modulation (Fig. 4A). Thus, by progressively reducing the global contribution from the *Hox* genes (k_{hox}), the resulting ω gradient became lower, but also shallower (fig. S6), reflecting the shallower wavelength gradients quantified from the mutants (Fig. 4B). In this way, the model was able to reproduce the observed smooth series of *Sox9* phenotypes in the $Gli3^{XtJ/XtJ}$ background—both the increased number of digits and the greater tendency for bifurcations (Fig. 3 and supplementary text). Although the observed reduction in wavelength was strongest in the absence of *Gli3*, the same trend was clearly apparent in the $Gli3^{+/+}$ and $Gli3^{+/XtJ}$ backgrounds (Fig. 4C and supplementary materials). In these cases, a reduced wavelength does not always produce a higher number of digits, because the AP width also decreases.

Our study highlighted a developmental delay in the appearance of the *Sox9* pattern (fig. S2) and a reduction in the PD width of the digit-forming region (fig. S3). Theoretical analysis revealed that both features are naturally predicted by modulating g_u in the model. The delayed patterning also supports the possible role of FGF signaling as a Turing modulator, as FGF4 treatment of micromass-cultured mesenchyme from limb buds sped up the appearance of the pattern (*25*). The simulated PD gradient of FGF signaling thus translates into a gradient of patterning speed, and further theoretical analysis revealed that this naturally predicts the progressive PD narrowing of the digital zone (fig. S6 and supplementary test). Below a certain *Hox* dose, the digital zone disappears entirely. Indeed, in triple mutants, no distinct digital condensations were scored, even at E13.5 (Fig. 3 and fig. S6).

In conclusion, our combination of genetics, quantitative analysis, and computer modeling reveals a missing piece of evidence for a Turing-type mechanism in digit patterning. Whereas numerous previous mutants have shown an abnormal digit number, evidence was lacking for a parameter that could smoothly tune digit wavelength. Our discovery and analysis of the smooth correlation between distal *Hox* gene number and digit wavelength provides this evidence. Additionally, the link between wavelength deregulation and the appearance of digit bifurcations also strongly supports the role of distal *Hox* genes as wavelength modulators of an intrinsic self-organizing Turing-type mechanism responsible for digit patterning. Our model predicts that overexpression of *Hox* genes should increase the digit wavelength, although this may require careful temporal examination at the time the Turing mechanism is operating and may have a subtle effect if *Hox* genes are normally expressed at saturating levels (*22*). The model makes no prediction about the temporal sequence of digit condensations along the AP axis. Also, the probability of bifurcations may be reduced in more extreme mutants (such as $Hoxa13^{+/-}$;$Hoxd^{Del11\text{-}13/Del11\text{-}13}$;$Gli3^{XtJ/XtJ}$) due to the narrower digital region. Additionally, our analysis suggests a role for *Gli3* in tuning the wavelength, but this observation is not as notable as the smooth trend seen in our distal *Hox* allelic series (Figs. 3 and 4C and supplementary materials).

Our results also permit a reassessment of distal *Hox* gene function in one of the most important vertebrate innovations: the fin-to-limb transition. The emerging consensus suggests that the genetic toolkit patterning fins and limbs is largely conserved, and the evolution of digits was driven by accumulated regulatory changes controlling the spatial and temporal deployment of that common toolkit (*27*–*32*). The reduction of the distal *Hox* gene number in the absence of *Gli3*, which renders Shh signaling irrelevant, resulted in mouse digits losing defining characteristics (pentadactyl constraint and segmented morphologies) and exhibiting patterns reminiscent of the endoskeleton patterns in chondrichthyan and basal actinopterygian fins (numerous, iterative, densely packed, infrequently segmented elements) (Fig. 5). Thus, our data provide evidence that an ancestral Turing-like mechanism patterning fins has been conserved in tetrapods and modified by the implementation of regulatory changes in the evolution of digits. In particular, our data suggest that the equilibrium resulting from the cross-regulation between Shh-Gli3 and distal *Hox* genes may have led to the stabilization of the pentadactyl state more than 360 million years ago.

References and Notes

1. M. F. Bastida, M. A. Ros, *Curr. Opin. Genet. Dev.* **18**, 374 (2008).
2. R. Zeller, J. López-Ríos, A. Zuniga, *Nat. Rev. Genet.* **10**, 845 (2009).
3. B. Wang, J. F. Fallon, P. A. Beachy, *Cell* **100**, 423 (2000).
4. Y. Litingtung, R. D. Dahn, Y. Li, J. F. Fallon, C. Chiang, *Nature* **418**, 979 (2002).
5. P. te Welscher *et al*., *Science* **298**, 827 (2002).
6. S. Kondo, T. Miura, *Science* **329**, 1616 (2010).
7. A. M. Turing, *Philos. Trans. R. Soc. London Ser. B.* **237**, 37 (1952).
8. S. A. Newman, H. L. Frisch, *Science* **205**, 662 (1979).
9. A. Gierer, H. Meinhardt, *Kybernetik* **12**, 30 (1972).
10. T. Miura, K. Shiota, G. Morriss-Kay, P. K. Maini, *J. Theor. Biol.* **240**, 562 (2006).
11. P. K. Maini, M. Solursh, *Int. Rev. Cytol.* **129**, 91 (1991).
12. S. A. Newman, *Bioessays* **18**, 171 (1996).
13. J. Zákány, D. Duboule, *Cell Tissue Res.* **296**, 19 (1999).
14. J. Zákány, M. Kmita, D. Duboule, *Science* **304**, 1669 (2004).
15. M. Kmita *et al*., *Nature* **435**, 1113 (2005).
16. Y. Chen *et al*., *Development* **131**, 2339 (2004).
17. M. Kmita, N. Fraudeau, Y. Hérault, D. Duboule, *Nature* **420**, 145 (2002).
18. C. Fromental-Ramain *et al*., *Development* **122**, 2997 (1996).
19. J. Zákány, C. Fromental-Ramain, X. Warot, D. Duboule, *Proc. Natl. Acad. Sci. U.S.A.* **94**, 13695 (1997).
20. A. P. Davis, M. R. Capecchi, *Development* **122**, 1175 (1996).
21. D. J. Goff, C. J. Tabin, *Development* **124**, 627 (1997).
22. V. Knezevic *et al*., *Development* **124**, 4523 (1997).
23. R. Sheth, M. F. Bastida, M. Ros, *Dev. Biol.* **310**, 430 (2007).
24. E. McGlinn *et al*., *Mech. Dev.* **122**, 1218 (2005).
25. T. Miura, P. K. Maini, *Bull. Math. Biol.* **66**, 627 (2004).
26. J. Lopez-Rios *et al*., *Dev. Cell* **22**, 837 (2012).
27. R. D. Dahn, M. C. Davis, W. N. Pappano, N. H. Shubin, *Nature* **445**, 311 (2007).
28. M. C. Davis, R. D. Dahn, N. H. Shubin, *Nature* **447**, 473 (2007).
29. R. Freitas, G. Zhang, M. J. Cohn, *PLoS ONE* **2**, e754 (2007).
30. J. M. Woltering, D. Duboule, *Dev. Cell* **18**, 526 (2010).
31. I. Schneider *et al*., *Proc. Natl. Acad. Sci. U.S.A.* **108**, 12782 (2011).
32. N. Shubin, C. Tabin, S. Carroll, *Nature* **457**, 818 (2009).

Acknowledgments: We thank D. Duboule and P. Chambon for the mutant mice, A. Munteanu for comments on the mathematical analysis, and M. Torres and M. Towers for critical reading of the manuscript. This work was supported by grant BFU2011-24972 from the Spanish Ministry of Science and Innovation to M.A.R. and by grant MOP-82880 from the Canadian Institutes of Health Research to M.K. R.S. was supported by a Formación Profesorado Universitario fellowship from the Spanish Ministry of Science and Innovation; L.M. was supported by a fellowship from the EMBL-CRG Systems Biology Program.

Supplementary Materials

www.sciencemag.org/cgi/content/full/338/6113/1476/DC1
Materials and Methods
Supplementary Text
Figs. S1 to S22
Tables S1 and S2
References (*33*–*46*)

2 July 2012; accepted 29 October 2012
10.1126/science.1226804

Hox Genes Regulate Digit Patterning by Controlling the Wavelength of a Turing-Type Mechanism

Rushikesh Sheth *et al.*

Science **338**, 1476 (2012);
DOI: 10.1126/science.1226804